Convergence of Sequential and Parallel One-Node CMFD Accelerations for Neutron Transport Analysis

HyeonTae Kim and Yonghee Kim*

** Department of Nuclear & Quantum Engineering, Korea Advanced Institute of Science and Technology (KAIST), Daejeon 34141, Republic of Korea, yongheekim@kaist.ac.kr*

INTRODUCTION

Parallel calculation method is gaining popularity in nuclear reactor physics, as computational loads of reactor problems have become more intensive. Hybrid CMFD (HCMFD) proposed in 2015 was reported to achieve over 95% of parallelism in various whole-core problems with high fidelity nodal expansion method [1,2], showing a huge potential of the parallel algorithm in reactor physics calculations. In the HCMFD, one-node CMFD and the conventional two-node CMFD were able to construct a global-local framework for the parallel calculation thanks to the non-overlapping scheme of the one-node CMFD. However, the one-node CMFD which is a key feature to achieve such high parallel efficiencies, was shown to be conditionally unstable, particularly for the problems with large optical thickness (σhp) and near unity scattering ratio ($c=\sigma_s/\sigma_t$) [3]. In order to solve this convergence issue, partial current-based CMFD (pCMFD) was applied in the one-node scheme, and shown to be unconditionally stable by numerical simulations [3]. In this study, Fourier analysis, which has been widely accepted for CMFD family's stability assessments [4], was used for analytic convergence studies for the suggested one-node CMFDs. Also, numerical simulations with S_{16} discrete ordinate method were conducted for comparison.

CMFD AND pCMFD WITH ONE-NODE KERNEL

For convergence analyses of the nonlinear acceleration methods, the 1-dimensional nuclear reactor core illustrated in Fig. 1 was considered. The reactor is divided into several coarse-mesh cells that are subdivided into *p* number of fine-meshes. For convenience, fine-mesh sizes were assumed to be identical throughout the core in this study.

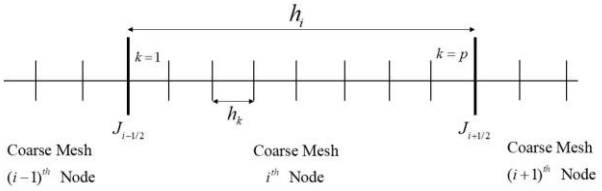

Fig. 1. 1- dimensional coarse/fine mesh divisions.

The one-node CMFD formulations and correction factors for the above core are as follows:

$$J^{-\varepsilon}_{i+1/2}=-\frac{2D_i}{h_i}\left(\phi_{i+1/2}-\bar{\phi}_i\right)-\frac{2\hat{D}^{-\varepsilon}_{i+1/2}}{h_i}\left(\phi_{i+1/2}+\bar{\phi}_i\right), \quad (1)$$

$$J^{+\varepsilon}_{i+1/2}=-\frac{2D_{i+1}}{h_{i+1}}\left(\bar{\phi}_{i+1}-\phi_{i+1/2}\right)+\frac{2\hat{D}^{+\varepsilon}_{i+1/2}}{h_{i+1}}\left(\bar{\phi}_{i+1}+\phi_{i+1/2}\right), \quad (2)$$

$$\hat{D}^{-\varepsilon}_{i+1/2}=-\frac{J^{l+1/2}_{i+1/2}h_i+2D_i\left(\phi^{l+1/2}_{i+1/2}-\bar{\phi}^{l+1/2}_i\right)}{2\left(\phi^{l+1/2}_{i+1/2}+\bar{\phi}^{l+1/2}_i\right)}, \quad (3)$$

$$\hat{D}^{+\varepsilon}_{i+1/2}=\frac{J^{l+1/2}_{i+1/2}h_{i+1}+2D_{i+1}\left(\bar{\phi}^{l+1/2}_{i+1}-\phi^{l+1/2}_{i+1/2}\right)}{2\left(\phi^{l+1/2}_{i+1/2}+\bar{\phi}^{l+1/2}_{i+1}\right)}. \quad (4)$$

The one-node pCMFD formulations and correction factors in the same core are as follows:

$$J^{+}_{i+1/2}=-\frac{\tilde{D}_i\left(\bar{\phi}_{i+1}-\bar{\phi}_i\right)+2\hat{D}^{+}_{i+1/2}\bar{\phi}_i}{2}, \quad (5)$$

$$J^{-}_{i+1/2}=\frac{\tilde{D}_i\left(\bar{\phi}_{i+1}-\bar{\phi}_i\right)+2\hat{D}^{-}_{i+1/2}\bar{\phi}_{i+1}}{2}, \quad (6)$$

$$\hat{D}^{+}_{i+1/2}=-\frac{2J^{+,l+1/2}_{i+1/2}+\tilde{D}_i\left(\bar{\phi}^{l+1/2}_{i+1}-\bar{\phi}^{l+1/2}_i\right)}{2\bar{\phi}^{l+1/2}_i}, \quad (7)$$

$$\hat{D}^{-}_{i+1/2}=\frac{2J^{-,l+1/2}_{i+1/2}-\tilde{D}_i\left(\bar{\phi}^{l+1/2}_{i+1}-\bar{\phi}^{l+1/2}_i\right)}{2\bar{\phi}^{l+1/2}_{i+1}}. \quad (8)$$

Coarse-mesh level

The neutron balance equation with respect to the i^{th} coarse-mesh node is:

$$J^{l+1}_{i+1/2}-J^{l+1}_{i-1/2}+\sum_k h_k\sigma_{r,ki}\phi^{l+1}_{ki}=\sum_k h_k q_k, \quad (9)$$

with the following angular discretization with discrete ordinate quadrature set of (μ_n,w_n):

$$J^{l+1}_{i+1/2}=\frac{1}{2}\sum_{n=1}^{N}w_n\mu_n\psi^{l+1}_{n,i+1/2}, \quad (10)$$

$$\phi^{l+1}_i=\frac{1}{2}\sum_{n=1}^{N}w_n\psi^{l+1}_{n,\mathrm{i}}. \quad (11)$$

Fine-mesh level

The neutron transport equation in 1-dimensional geometry is as follows:

$$\mu\frac{d}{dx}\psi^{l+1/2}(x,\mu)+\sigma_t(x)\psi^{l+1/2}(x,\mu)=\sigma_s(x)\phi^{l}(x)+q(x). \quad (12)$$

Discretizing the transport equation for the sequential algorithm using the quadrature set and diamond rule results:

$$\mu_n \frac{\psi^{l+1/2}_{n,k+1/2} - \psi^{l+1/2}_{n,k-1/2}}{h_k} + \sigma_t \frac{\psi^{l+1/2}_{n,k+1/2} + \psi^{l+1/2}_{n,k-1/2}}{2} = \sigma_s \phi^l_k + Q, \quad (13)$$

$$\phi^{l+1/2}_k = \frac{1}{2}\sum_{n=1}^{N} w_n \frac{\psi^{l+1/2}_{n,k+1/2} + \psi^{l+1/2}_{n,k-1/2}}{2}. \quad (14)$$

Flux modulation

The coarse-mesh level diffusion solution can accelerate local source iteration through the flux modulation step. Here, local flux shape is multiplied by the ratio of coarse-mesh average flux (Φ_i) :

$$\phi^{l+1}_k = \phi^{l+1/2}_k \frac{\Phi^{l+1}_i}{\Phi^{l+1/2}_i}. \quad (15)$$

FOURIER CONVERGENCE ANALYSIS

In this paper, Fourier analysis was used for analytic convergence studies for the one-node CMFD and the one-node pCMFD. In the following sections, the Fourier analysis equations and their short derivations for determining spectral radius are described both for the sequential and the parallel algorithm. In the analyses, infinite homogeneous material with uniform fixed source distribution (Q) was considered.

In order to carry out the Fourier analysis, the nonlinear CMFD equations must be linearized using the following expressions:

$$\psi^{l+1/2}_{m,i+1/2} = \frac{Q}{\sigma_a}\left(1 + \varepsilon \xi^{l+1/2}_{m,i+1/2}\right), \quad (16\text{-a})$$

$$\bar{\phi}^{l+1/2}_i = \frac{Q}{\sigma_a}\left(1 + \varepsilon \zeta^{l+1/2}_i\right), \quad (16\text{-b})$$

$$\bar{\phi}^{l}_i = \frac{Q}{\sigma_a}\left(1 + \varepsilon \zeta^{l}_i\right). \quad (16\text{-c})$$

The Equation (16) describes the reactor parameters at l^{th} iteration step with corresponding errors. With the given problem condition, the scalar flux throughout the core should be Q/σ_a, and ε represents an error at the iteration step. By substituting Eq. (16) into the CMFD equations (Eq. (9), (13), (14), and (15)) and keeping $O(\varepsilon)$ terms, we can obtain linearized CMFD equations of which we can apply the Fourier analysis.

Sequential algorithm

The linearized one-node CMFD equations from Eqs. (9), (13), (14), and (15) are as follows:

$$\begin{aligned} &\frac{1}{3hp\sigma_t}\zeta^{l+1/2}_{i-1} - \frac{2}{3hp\sigma_t}\zeta^{l+1/2}_{i} + \frac{1}{3hp\sigma_t}\zeta^{l+1/2}_{i+1} \\ &-h\sigma_t \sum_k \zeta^{l+1/2}_k + h\sigma_s \sum_k \zeta^{l}_k \\ &= \frac{1}{3hp\sigma_t}\zeta^{l+1}_{i-1} + \left(-\frac{2}{3hp\sigma_t} - hp\sigma_r\right)\zeta^{l+1}_i + \frac{1}{3hp\sigma_t}\zeta^{l+1}_{i+1}, \end{aligned} \quad (17)$$

$$\mu_n \frac{\xi^{l+1/2}_{n,k+1/2} - \xi^{l+1/2}_{n,k-1/2}}{h} + \sigma_t \frac{\xi^{l+1/2}_{n,k+1/2} + \xi^{l+1/2}_{n,k-1/2}}{2} = \sigma_s \zeta^l_k, \quad (18)$$

$$\zeta^{l+1/2}_k = \frac{1}{2}\sum_{n=1}^{N} w_n \frac{\xi^{l+1/2}_{n,k+1/2} + \xi^{l+1/2}_{n,k-1/2}}{2}, \quad (19)$$

$$\zeta^{l+1}_k - \zeta^{l+1/2}_k = \zeta^{l+1}_i - \zeta^{l+1/2}_i. \quad (20)$$

Now, by adopting the following Fourier ansatz, we can evaluate a spectral radius which is a convergence factor.

$$\zeta^l_i = \omega^l A \exp(j\lambda x_i), \quad (21\text{-a})$$

$$\zeta^l_k = \omega^l A_k \exp(j\lambda x_k), \quad (21\text{-b})$$

$$\zeta^{l+1/2}_i = \omega^l B \exp(j\lambda x_i), \quad (21\text{-c})$$

$$\zeta^{l+1/2}_k = \omega^l B_k \exp(j\lambda x_k), \quad (21\text{-d})$$

$$\xi^{l+1/2}_{k+1/2} = \omega^l a_{n,k} \exp(j\lambda x_{k+1/2}). \quad (21\text{-e})$$

Parallel algorithm

The Fourier analysis for the parallel algorithm is much more complicated compared to the sequential algorithm, and it is first demonstrated by Kelley and Larsen [5]. In the local calculation, angular fluxes from the previous iteration step are used for boundary conditions. Therefore, fine-mesh cells at the end of the coarse-mesh cell should be considered in a different way. The modified local neutron transport equations are as follows:

For $k = 1$ and $\mu_n > 0$,

$$\mu_n \frac{\psi^{l+1/2}_{n,k+1/2} - \psi^{l}_{n,k-1/2}}{h} + \sigma_t \frac{\psi^{l+1/2}_{n,k+1/2} + \psi^{l}_{n,k-1/2}}{2} = \sigma_s \phi^l_k + Q, \quad (22\text{-a})$$

For $k = p$ and $\mu_n < 0$,

$$\mu_n \frac{\psi^{l}_{n,k+1/2} - \psi^{l+1/2}_{n,k-1/2}}{h} + \sigma_t \frac{\psi^{l}_{n,k+1/2} + \psi^{l+1/2}_{n,k-1/2}}{2} = \sigma_s \phi^l_k + Q, \quad (22\text{-b})$$

Otherwise,

$$\mu_n \frac{\psi^{l+1/2}_{n,k+1/2} - \psi^{l+1/2}_{n,k-1/2}}{h} + \sigma_t \frac{\psi^{l+1/2}_{n,k+1/2} + \psi^{l+1/2}_{n,k-1/2}}{2} = \sigma_s \phi^l_k + Q. \quad (22\text{-c})$$

The diamond rule for the parallel algorithm is also modified as:

For $k = 1$ and $\mu_n > 0$,

$$\phi_k^{l+1/2} = \frac{1}{2}\left[\sum_{n=1}^{N/2} w_n \frac{\psi_{n,k+1/2}^{l+1/2} + \psi_{n,k-1/2}^{l+1/2}}{2} + \sum_{n=N/2+1}^{N} w_n \frac{\psi_{n,k+1/2}^{l+1/2} + \psi_{n,k-1/2}^{l}}{2}\right], \quad (23\text{-a})$$

For $k = p$ and $\mu_n < 0$,

$$\phi_k^{l+1/2} = \frac{1}{2}\left[\sum_{n=1}^{N/2} w_n \frac{\psi_{n,k+1/2}^{l} + \psi_{n,k-1/2}^{l+1/2}}{2} + \sum_{n=N/2+1}^{N} w_n \frac{\psi_{n,k+1/2}^{l+1/2} + \psi_{n,k-1/2}^{l+1/2}}{2}\right], \quad (23\text{-b})$$

Otherwise,

$$\phi_k^{l+1/2} = \frac{1}{2}\sum_{n=1}^{N} w_n \frac{\psi_{n,k+1/2}^{l+1/2} + \psi_{n,k-1/2}^{l+1/2}}{2}. \quad (23\text{-c})$$

By substituting Eq. (21) into the Eq. (22) and (23), we can get linearized local equations for the parallel algorithm.

Local transport equations

For $k = 1$ and $\mu_n > 0$,

$$\mu_n \frac{\xi_{n,k+1/2}^{l+1/2} - \xi_{n,k-1/2}^{l}}{h} + \sigma \frac{\xi_{n,k+1/2}^{l+1/2} + \xi_{n,k-1/2}^{l}}{2} = \sigma_s \zeta_k^l, \quad (24\text{-a})$$

For $k = p$ and $\mu_n < 0$,

$$\mu_n \frac{\xi_{n,k+1/2}^{l} - \xi_{n,k-1/2}^{l+1/2}}{h} + \sigma \frac{\xi_{n,k+1/2}^{l} + \xi_{n,k-1/2}^{l+1/2}}{2} = \sigma_s \zeta_k^l, \quad (24\text{-b})$$

Otherwise,

$$\mu_n \frac{\xi_{n,k+1/2}^{l+1/2} - \xi_{n,k-1/2}^{l+1/2}}{h} + \sigma \frac{\xi_{n,k+1/2}^{l+1/2} + \xi_{n,k-1/2}^{l+1/2}}{2} = \sigma_s \zeta_k^l. \quad (24\text{-c})$$

Diamond rule

For $k = 1$ and $\mu_n > 0$,

$$\zeta_k^{l+1/2} = \frac{1}{2}\left[\sum_{n=1}^{N/2} w_n \frac{\xi_{n,k+1/2}^{l+1/2} + \xi_{n,k-1/2}^{l+1/2}}{2} + \sum_{n=N/2+1}^{N} w_n \frac{\xi_{n,k+1/2}^{l+1/2} + \xi_{n,k-1/2}^{l}}{2}\right], \quad (25\text{-a})$$

For $k = p$ and $\mu_n < 0$,

$$\zeta_k^{l+1/2} = \frac{1}{2}\left[\sum_{n=1}^{N/2} w_n \frac{\xi_{n,k+1/2}^{l} + \xi_{n,k-1/2}^{l+1/2}}{2} + \sum_{n=N/2+1}^{N} w_n \frac{\xi_{n,k+1/2}^{l+1/2} + \xi_{n,k-1/2}^{l+1/2}}{2}\right], \quad (25\text{-b})$$

Otherwise,

$$\zeta_k^{l+1/2} = \frac{1}{2}\sum_{n=1}^{N} w_n \frac{\xi_{n,k+1/2}^{l+1/2} + \xi_{n,k-1/2}^{l+1/2}}{2}. \quad (25\text{-c})$$

The coarse-mesh diffusion equation for the one-node CMFD is also modified as:

$$\begin{aligned} &\frac{1}{3hp\sigma_t}\zeta_{i-1}^{l+1/2} - \frac{2}{3hp\sigma_t}\zeta_i^{l+1/2} + \frac{1}{3hp\sigma_t}\zeta_{i+1}^{l+1/2} \\ &-h\sigma_t \sum_k \zeta_k^{l+1/2} + h\sigma_s \sum_k \zeta_k^{l} \\ &-\frac{1}{2}\left[\sum_{\mu_n<0} w_n\mu_n\left(\xi_{n,i+1/2}^{l} - \xi_{n,i+1/2}^{l+1/2}\right) + \sum_{\mu_n>0} w_n\mu_n\left(\xi_{n,i-1/2}^{l+1/2} - \xi_{n,i-1/2}^{l}\right)\right] \\ &= \frac{1}{3hp\sigma_t}\zeta_{i-1}^{l+1} + \left(-\frac{2}{3hp\sigma_t} - hp\sigma_r\right)\zeta_i^{l+1} + \frac{1}{3hp\sigma_t}\zeta_{i+1}^{l+1}, \end{aligned} \quad (26)$$

while the flux modulation equation stays the same. The coarse-mesh equation for the one-node pCMFD can also be obtained in the same way. By applying the same Fourier ansatz into Eqs. (24) to (26), we can get a formulation for spectral radius evaluation, though it is very complex. The detailed expression is not described here for brevity.

RESULTS

In this section, results from the Fourier analysis and numerical simulation are presented. For the numerical simulation, 1-dimensional 1000cm slab reactor with flat fixed source of $Q = 1.0\ \#/cm^3\,\text{sec}$ was considered. Here, vacuum boundary conditions were imposed at each end. The tests were conducted for two scattering ratio values, and the spectral radius is plotted with respect to the coarse-mesh optical thickness. Figures 2 and 3 illustrate spectral radius behaviors of the one-node CMFD and the one-node pCMFD in the sequential algorithm. The one-node CMFD's instability was predicted from the Fourier analysis and also shown by the numerical simulation for large scattering ratio.

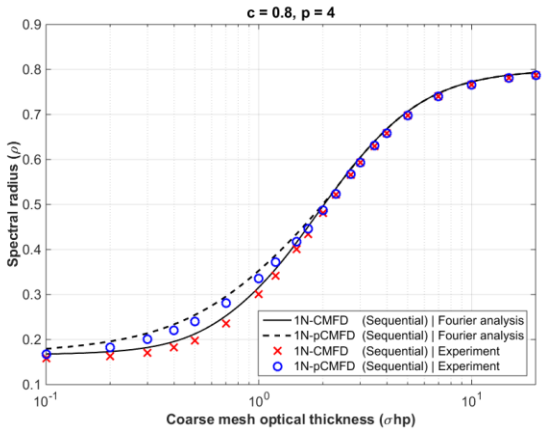

Fig. 2. Spectral radius of the sequential algorithm for the scattering ratio of 0.8 and coarse-mesh division into 4 equal fine-meshes

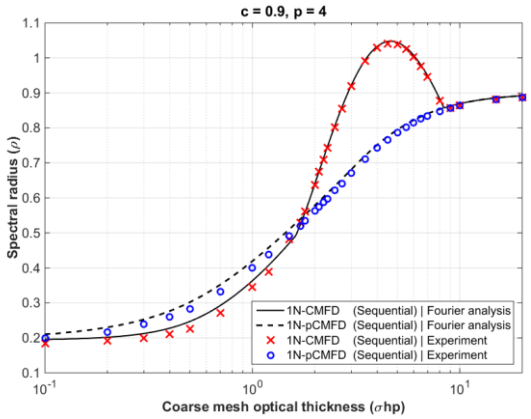

Fig. 3. Spectral radius of the sequential algorithm for the scattering ratio of 0.9 and coarse-mesh division into 4 equal fine-meshes

In the parallel algorithm, the instability was also found for the case with large scattering ratio. The Fourier analyses were able to predict spectral radii for the two one-node CMFDs. A noticeable difference between the sequential and the parallel algorithm's convergences is the presence of a special optical thickness giving a minimum spectral ratio. For the parallel algorithm, the convergence became worse in optically thin region. Since the parallel algorithm uses previous iteration's information for boundary conditions, the convergence is essentially less than the sequential algorithm. As we place more coarse-mesh cells, the effect from the previous iterations would be increased. In optically thin region, this effect dominates the convergence, therefore shows slower convergence. Also, the results from the Fourier analysis and the numerical simulation showed noticeable discrepancy in the optically thin region. Since we imposed vacuum boundary conditions for the numerical simulation, the correction factor formulation was different at the two boundaries. The limitation of this convergence analysis caused from the infinite geometry assumption is shown here.

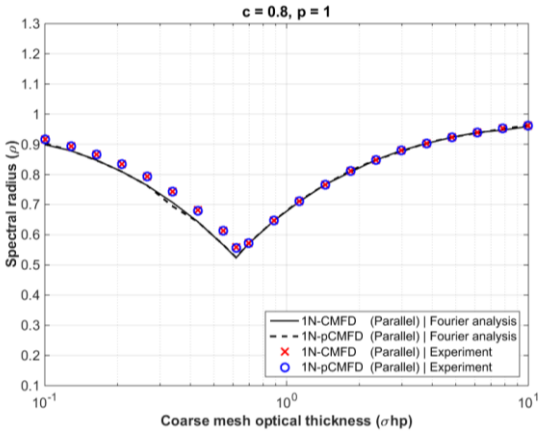

Fig. 4. Spectral radius of the parallel algorithm for the scattering ratio of 0.8 and coarse-mesh division into a single fine-mesh

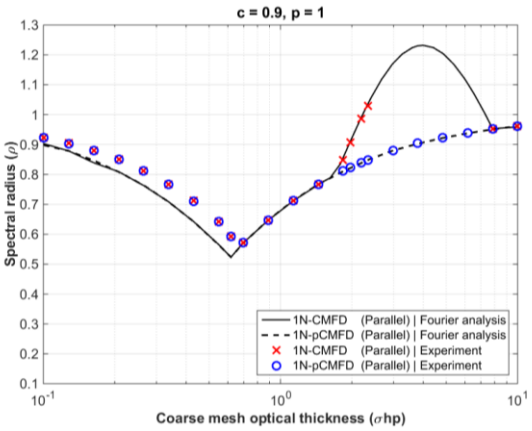

Fig. 5. Spectral radius of the parallel algorithm for the scattering ratio of 0.9 and coarse-mesh division into a single fine-mesh

SUMMARY

In this study, the convergence rates of the two one-node CMFDs were evaluated for the sequential and the parallel algorithm. The results from the Fourier analyses and the numerical simulations showed good agreement, except for the parallel algorithm in optically thin region as an effect of boundary condition is appeared. The one-node CMFD showed instabilities in both sequential and the parallel algorithm with large scattering ratio. On the other hand, the one-node pCMFD was everywhere stable according to this study. From this result, the one-node pCMFD was found to be a better option for the parallel algorithm.

ACKNOWLEDGEMENT

This work was supported by the National Research foundation of Korea Grant funded by the Korean government NRF-2016R1A5A1013919

REFERENCES

1. S.H. Song et al., An Efficient One-Node and Two-Node Hybrid CMFD Method for Pin-by-Pin Reactor Analysis, KNS Autumn Meeting, Gyeongju, Korea (2015).
2. Jaeha Kim and Y. Kim, Performance of the HCMFD-based Pin-wise 3D Core Analysis in Big PWRs, Proc. Reactor Physics Asia 2017, Chengdu, China (2017).
3. H. Kim and Y. Kim, Convergence Analyses of 1-Node and 2-Node CMFD Schemes for the Neutron Transport, KNS Autumn Meeting, Gyeongju, Korea (2015).
4. N.Z. Cho and C.J. Park, A Comparison of Coarse Mesh Rebalance and Coarse Mesh Finite Difference Accelerations for the Neutron Transport Calculations, Proc. M&C 2003, Gatlinburg, Tennessee, USA (2003).
5. B.W. Kelley and E.W. Larsen, CMFD Acceleration of Spatial Domain-Decomposed Neutron Transport Problems, PHYSOR, Knoxville, Tennessee, USA (2012)